

Beaming electromagnetic (or heat-flux) instabilities from the interplay with the electron temperature anisotropies

S. M. Shaaban,^{1,2, a)} M. Lazar,^{1,3} P. H. Yoon,^{4,5} and S. Poedts¹

¹⁾Centre for Mathematical Plasma-Astrophysics, KU Leuven, Celestijnenlaan 200B, 3001 Leuven, Belgium

²⁾Theoretical Physics Research Group, Physics Dept., Faculty of Science, Mansoura University, 35516 Mansoura, Egypt

³⁾Institut für Theoretische Physik, Lehrstuhl IV: Weltraum- und Astrophysik, Ruhr-Universität Bochum, D-44780 Bochum, Germany

⁴⁾Institute for Physical Science and Technology, University of Maryland, College Park, MD 20742, USA

⁵⁾Korea Astronomy and Space Science Institute, Daejeon 34055, Korea School of Space Research, Kyung Hee University, Yongin, Gyeonggi 17104, Korea

(Dated: 16 July 2018; Revised -)

In space plasmas kinetic instabilities are driven by the beaming (drifting) components and/or the temperature anisotropy of charged particles. The heat-flux instabilities are known in the literature as electromagnetic modes destabilized by the electron beams (or strahls) aligned to the interplanetary magnetic field. A new kinetic approach is proposed here in order to provide a realistic characterization of heat-flux instabilities under the influence of electrons with temperature anisotropy. Numerical analysis is based on the kinetic Vlasov-Maxwell theory for two electron counter-streaming (core and beam) populations with temperature anisotropies, and stationary, isotropic protons. The main properties of electromagnetic heat-flux instabilities are found to be markedly changed by the temperature anisotropy of electron beam $A_b = T_{\perp}/T_{\parallel} \neq 1$, leading to stimulation of either the whistler branch if $A_b > 1$, or the firehose branch for $A_b < 1$. For a high temperature anisotropy whistlers switch from heat-flux to a standard regime, when their instability is inhibited by the beam.

I. INTRODUCTION

Collision-poor plasmas from space are highly susceptible to the instabilities driven by the kinetic anisotropies of plasma particles. Thus, the electron strahls, or beaming populations, which carry the electron heat-flux in the solar wind, are often associated with enhanced electromagnetic (EM) fluctuations (Lengyel-Frey et al., 1996; Lin et al., 1998; Lacombe et al., 2014) presumably attributed to the so-called heat-flux instabilities (Gary et al., 1975). Contrary to a magnetic focusing predicted by the theory, the observations show that strahls lose intensity and become wider with heliospheric distance (Maksimovic et al., 2005; Štverák et al., 2009). In the absence of collisions between particles only the self-generated instabilities can be responsible for this degradation (Pagel et al., 2007; Saito and Gary, 2007; Gary and Saito, 2007; Vocks et al., 2005). These evidences explain the increasing interest for the heat-flux instabilities (Saeed et al., 2017a,b; Shaaban et al., 2018a), and understanding their role in this context implies a detailed examination in conditions specific to solar wind.

The heat-flux instabilities are highly conditioned by the electron beam, and, depending on the relative beam velocity, two distinct branches can be destabilized. Whistlers with a right-handed (RH) circular polarization (in direction of the uniform magnetic field) are excited

by a less energetic beam with velocity lower than thermal speed. Growth rates of the whistler heat flux instability (WHFI) show a non-uniform variation, increasing and then decreasing with increasing the beaming velocity (Gary, 1985; Shaaban et al., 2018a). In the second branch the left handed (LH) firehose heat flux instability (FHFI) (Gary, 1985) is excited by a more energetic beam, with growth rates increasing monotonically with increasing the beam velocity (Gary, 1985; Saeed et al., 2017b; Shaaban et al., 2018a). Recently, Shaaban et al. (2018a) have derived the beam velocity thresholds for each of these two instabilities in the absence of temperature anisotropy, and described the intermediary regime of transition, where both heat-flux instabilities may co-exist and compete to each other. It has also been shown that effective (counter-)beaming anisotropy is reduced by the suprathermal electrons present in space plasmas, which implies stimulation of the unstable whistlers but inhibition of the firehose instability.

Beams or counter-beaming populations of electrons are ubiquitous in space plasmas, e.g., during fast winds and coronal mass ejections, and their kinetic implications cannot be isolated from the effects of temperature anisotropies, if both these two sources of free energy are present (Štverák et al., 2008; Viñas et al., 2010). Here we indeed show that all known properties of the heat-flux and temperature anisotropy-driven instabilities may be significantly altered by the interplay of beaming electrons and their temperature anisotropy, i.e., $T_{\perp} \neq T_{\parallel}$. In fact, in such a complex (but realistic) scenario we deal with two distinct triggers of the same unstable modes.

^{a)}Electronic mail: shaaban.mohammed@kuleuven.be

The heat-flux instabilities described above may interplay with the common whistler instability (WI) driven by anisotropic electrons with $T_{\perp} > T_{\parallel}$ (Gary and Wang, 1996; Štverák et al., 2008; Lazar et al., 2018), or the well-known firehose instability (FHI) excited by the electrons with an opposite anisotropy $T_{\perp} < T_{\parallel}$ (Paesold and Benz, 1999; Štverák et al., 2008; Lazar et al., 2018). Recent studies have investigated these regimes for low-beta ($\beta \leq 0.4$) electrons, and found that WI is inhibited by the beam (growth rates decrease with increasing the beam velocity), while FHI is insensitive to a temperature anisotropy $T_{\perp} > T_{\parallel}$ of the beam (Saeed et al., 2017b). In an attempt to make a reliable distinction between the heat-flux and temperature anisotropy instabilities, our present study provides an extended comparative analysis, including the solar wind high-beta ($\beta \geq 1$) conditions, where kinetic instabilities are expected to be more operative. Suprathermal populations are not considered in the present analysis, with the express intention to isolate and describe only the instabilities resulting from the cumulative effects of electron beams and temperature anisotropy.

In Section II we describe the distribution models for the electrons and protons, and derive the general dispersion relation for the EM modes, which incorporates the instability cumulative effects of anisotropic electrons. Whistlers are studied in sec. III and firehose instability in sec. IV, and then in sec. V we provide a comparative study of the instability threshold conditions for different regimes, e.g., WHFI, FHI, WI and FHI, as resulting from the interplay of electron beam and temperature anisotropy. Section VI summarizes the results obtained in this work with discussions and conclusions.

II. DISPERSION RELATIONS

We consider a collisionless quasi-neutral electron-proton plasma with two populations of electrons, namely, the core (subscript $a = c$) and the beam (subscript $a = b$), counterstreaming in the protons' frame

$$f_e(v_{\perp}, v_{\parallel}) = \eta f_c(v_{\perp}, v_{\parallel}) + \delta f_b(v_{\perp}, v_{\parallel}), \quad (1)$$

where $\eta = n_c/n_e$ and $\delta = 1 - \eta$ are relative number densities satisfying neutrality of charge of the electrons (subscript e) and protons (subscript p), $n_e = n_c + n_b = n_p$. Each component is a drifting bi-Maxwellian

$$f_a(v_{\perp}, v_{\parallel}) = \frac{\pi^{-3/2}}{\alpha_{a,\perp}^2 \alpha_{a,\parallel}} \exp \left[-\frac{v_{\perp}^2}{\alpha_{a,\perp}^2} - \frac{(v_{\parallel} - U_a)^2}{\alpha_{a,\parallel}^2} \right] \quad (2)$$

where drifting velocities U_a are directed along the magnetic field and satisfy a zero net current condition $n_c U_c + n_b U_b = 0$. Thermal velocities $\alpha_{a,\parallel} = \sqrt{2k_B T_{a,\parallel}/m_a}$ and $\alpha_{a,\perp} = \sqrt{2k_B T_{a,\perp}/m_a}$, are defined in terms of the anisotropic temperature components, parallel (T_{\parallel}) and perpendicular (T_{\perp}) to the ambient magnetic field \mathbf{B} . If protons are bi-Maxwellian, the

linear dispersion relations describing the parallel electromagnetic modes read (Gary, 1985)

$$\frac{c^2 k^2}{\omega^2} = 1 + \sum_{a=e,c,b} \frac{\omega_{p,a}^2}{\omega^2} [\xi_a Z(\xi_a^{\pm}) + \Lambda_a \{1 + \xi_a^{\pm} Z(\xi_a^{\pm})\}] \quad (3)$$

where c is the speed of light, ω is the wave frequency, k is the wave number, $\omega_{p,a}^2 = 4\pi n_a e^2/m_a$ is the plasma frequency, \pm distinguish between the circular right-handed (RH) and left-handed (LH) polarizations, respectively, $\Lambda_a = A_a - 1$, in terms of temperature anisotropy $A_a = T_{a,\perp}/T_{a,\parallel}$, $\xi_a = (\omega - kU_a)/(k\alpha_{a,\parallel})$, and

$$Z(\xi_a^{\pm}) = \frac{1}{\pi^{1/2}} \int_{-\infty}^{\infty} \frac{\exp(-x^2)}{x - \xi_a^{\pm}} dt, \quad \Im(\xi_a^{\pm}) > 0 \quad (4)$$

is the plasma dispersion function (Fried and Conte, 1961) of argument

$$\xi_a^{\pm} = \frac{\omega \pm \Omega_a - kU_a}{k\alpha_{a,\parallel}}.$$

For isotropic protons, we can rewrite (3)

$$\begin{aligned} & \frac{\tilde{w}}{\tilde{k}\sqrt{\mu\beta_p}} Z\left(\frac{\mu\tilde{w} \pm 1}{\tilde{k}\sqrt{\mu\beta_p}}\right) + \eta \left[\Lambda_c + \frac{(\Lambda_c + 1)(\tilde{w} + u_c \tilde{k}) \mp \Lambda_c}{\tilde{k}\sqrt{\beta_c}} \right. \\ & \times Z\left(\frac{\tilde{w} \mp 1 + u_c \tilde{k}}{\tilde{k}\sqrt{\beta_c}}\right) \left. \right] + \delta \left[\Lambda_b + \frac{(\Lambda_b + 1)(\tilde{w} - u_b \tilde{k}) \mp \Lambda_b}{\tilde{k}\sqrt{\beta_b}} \right. \\ & \times Z\left(\frac{\tilde{w} \mp 1 - u_b \tilde{k}}{\tilde{k}\sqrt{\beta_b}}\right) \left. \right] = \tilde{k}^2 \end{aligned} \quad (5)$$

in terms of the normalized quantities, $\tilde{k} = kc/\omega_{p,e}$, $\tilde{w} = \omega/|\Omega_e|$, the proton-electron mass ratio $\mu = m_p/m_e$, the plasma beta for the population of sort a , $\beta_a = 8\pi n_a k_B T_{a,\parallel}/B^2$, and relative velocities of the beam and core components, $u_b = U_b \omega_{p,e}/(c\Omega_e)$ and $u_c = \delta u_b/(1 - \delta)$, respectively.

Plasma parameters used in the numerical calculations are given in Table I, unless otherwise specified. These parameters are inspired from the solar wind observations providing electron data from different heliocentric distances. Relevant are the electron data making distinction between core and beaming (strahl) components, see the density contrasts in Štverák et al. (2009) (Figs. 4

TABLE I. Parameters for the j -component of electrons

	Beam electrons (b)	Core electrons (c)	Ions (i)
n_j/n_i	0.05	0.95	1.0
$T_{j,\parallel}/T_{i,\parallel}$	10.0	1.0	1.0
m_j/m_i	1/1836	1/1836	1.0
$T_{j,\perp}/T_{j,\parallel}$	$\neq 1.0$	$\neq 1.0$	1.0

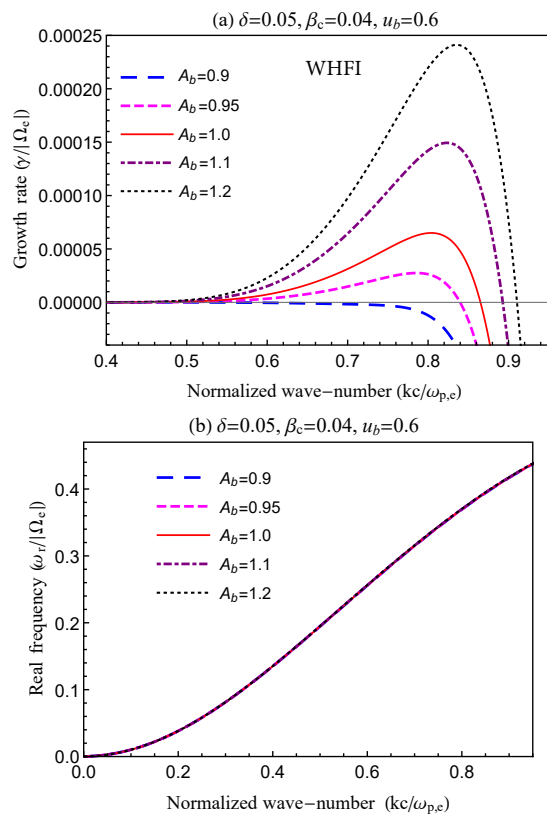


FIG. 1. WHFI: Effects of the beam anisotropy A_b on the growth rates (panel a) and wave frequencies (panel b). The plasma parameters are mentioned in each panel velocity.

and 8), which suggest an average (representative) value $\delta = n_b/n_0 = 0.05$. Presuming that strahl and halo electrons comprise the main source of the heat flux transport in the solar wind, for the beam-core temperature contrast the observations estimate a variation between 3 and 13 along the heliocentric distance with an increasing tendency during the fast winds (Pilipp et al., 1987; Viñas et al., 2010; Pierrard et al., 2016). In this case we assume $T_{b,\parallel}/T_{c,\parallel} = 10$. Seeking generalization, for the temperature anisotropy, which is a key parameter in this study, we adopt moderate values typically reported in the solar wind (Pilipp et al., 1987; Phillips et al., 1989; Štverák et al., 2008; Pierrard et al., 2016). For the beam velocity values are chosen to ensure conditions for both the WHFI and FHFI, which may also be relevant for the beaming electrons in space plasmas (Pulupa et al., 2014).

III. UNSTABLE WHISTLER MODES

We start the analysis with the dispersive characteristics of the whistler modes driven unstable by the interplay of the beam-core counter-streaming electrons and their temperature anisotropies. These are solutions of the dispersion relation (3) for the RH modes with ξ_p^+ . The less energetic beams are susceptible to the whistler heat

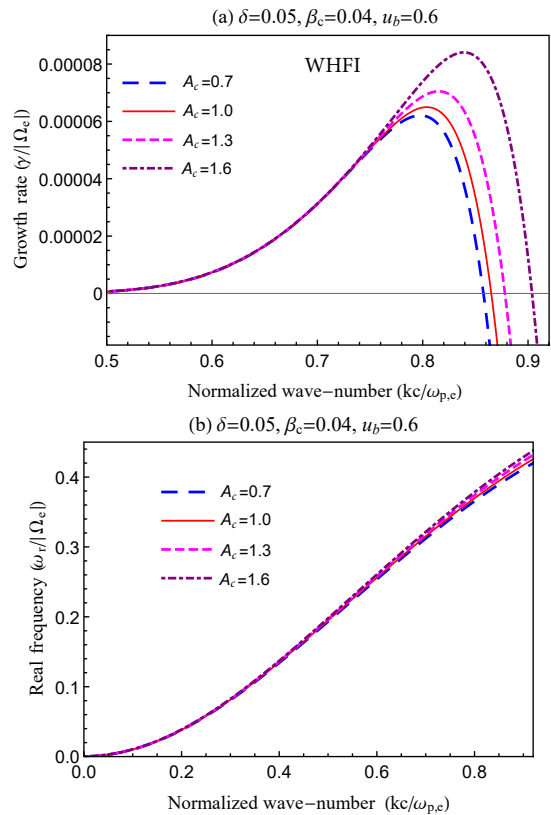


FIG. 2. WHFI: Effects of the core anisotropy A_c on the growth rates (panel a) and wave frequencies (panel b). The plasma parameters are mentioned in each panel.

flux instability (WHFI) (Shaaban et al., 2018a), which is examined in Figures 1 and 2 for the following plasma parameters $\delta = 0.05$, $\beta_c = \beta_p = 0.04$, $u_b = 0.6$. In Figure 1 we isolate the effects of the beam anisotropy by considering isotropic core with $A_c = 1.0$, and show the influence of the beam anisotropy $A_b = 0.9, 0.95, 1.0, 1.1, 1.2$ on the growth rates (panel a) and wave-frequencies (panel b) of WHFI. Growth rates are markedly enhanced by increasing the temperature anisotropy in perpendicular direction, $A_b > 1$, and are inhibited by an opposite anisotropy in parallel direction, $A_b < 1$. The corresponding wave-frequencies remain unaffected by the variation of the beam temperature anisotropy. These unstable solutions are derived for relatively low anisotropies of the beam ($0.9 \leq A_b \leq 1.2$), and a low plasma beta of the core $\beta_c = 0.04$, to avoid the whistler or firehose instability effects driven by the temperature anisotropies. For higher anisotropies of the beam $A_b > 1.2$ whistlers exhibit significant growth rates characteristic to the whistler instability (WI) driven by the temperature anisotropy, and it becomes difficult to distinguish between the WHF and WI regimes, as discussed later in Figures 4. In Figure 2 we assume an isotropic beam ($A_b = 1$) and outline the effect of the core anisotropy $A_c = 0.7, 1.0, 1.3, 1.6$ on the growth rates (panel a) and wave-frequencies (panel b) of WHFI. The growth rates change only slightly, being

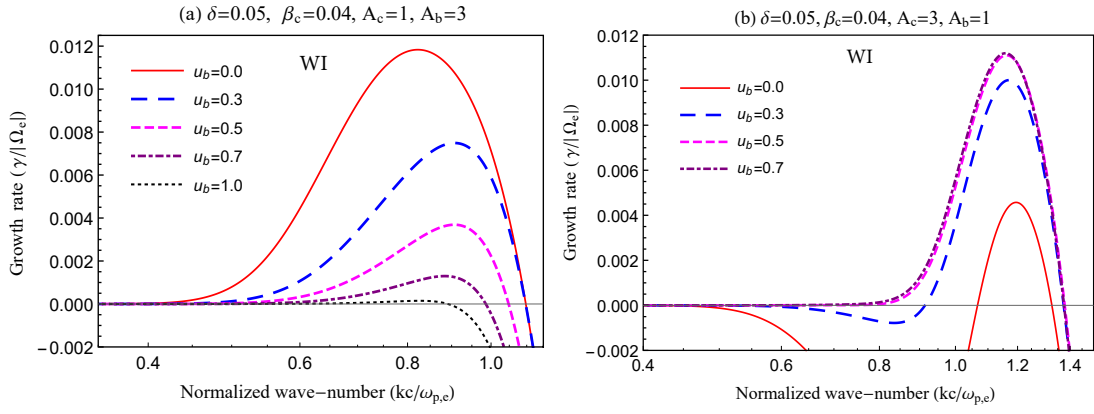


FIG. 3. WI: Effects of the beam velocity u_b on the growth rates of the WI driven either by an anisotropic beam $A_b = 3.0$ (panel a) or by an anisotropic core $A_c = 3.0$ (panel b). The other plasma parameters are mentioned in each panel.

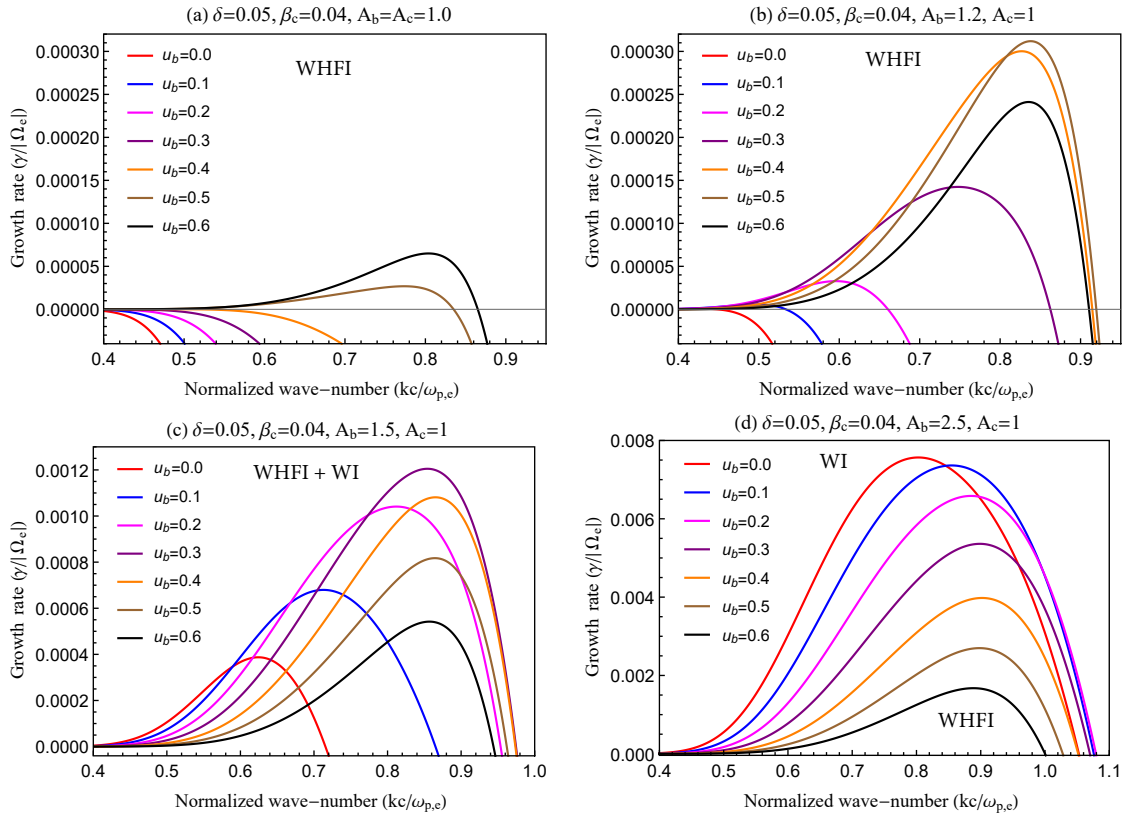


FIG. 4. Effect of the of the beam velocity u_b on the cumulative whistler instabilities for beam anisotropies $A_b = 1.0$ (panel a), $A_b = 1.2$ (panel b), $A_b = 1.5$ (panel c), $A_b = 2.5$ (panel d). The plasma parameters are mentioned in each panel.

enhanced by the core anisotropy in perpendicular direction $A_c > 1$, but inhibited by an opposite anisotropy in parallel direction $A_c < 1$. Clearly, the anisotropic beam has a higher influence on the instability: for $A_b = 1.1$ maximum growth rate in Figure 1 is three times higher than that obtained for $A_c = 1.6$ in Figure 2. For reference, the growth rates for isotropic isotropic temperatures $A_b = A_c = 1$, are displayed in both figures with red solid lines.

The temperature anisotropy driven instabilities are usually studied in the absence of beaming components. Figure 3 shows the effect of beaming velocity u_b on the WI driven by a higher temperature anisotropy, for $\delta = 0.05$ and $\beta_c = \beta_p = 0.04$. When WI is driven by anisotropic beam with $A_b = 3.0$ (panel a), the effective anisotropy diminishes with increasing the beam speed u_b and the instability is inhibited, reducing growth rates and the intervals of unstable wave-numbers. By con-

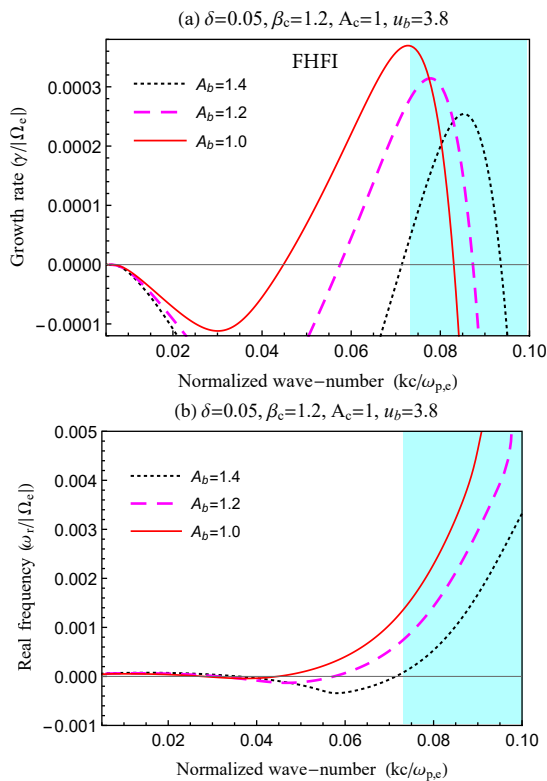


FIG. 5. FHF: Effect of beam anisotropy $A_b > 1$ on the growth rates (panel a) and wave frequency (panel b).

trast, growth rates driven by the anisotropic core with $A_c = 3.0$ (panel b) are enhanced by increasing u_b , and saturate for $u_b \geq 0.5$, resembling a regime characteristic to WHFI. The wave frequency (not shown here) only slightly decreases by increasing u_b . WHFI has dispersive characteristics similar to WI. Both instabilities are driven by resonant electrons and display maximum growth rates in directions parallel to the background magnetic field (when the modes are right-hand circularly polarized) (Gary, 1993; Lazar et al., 2018). However, WHFI and WI represent two distinct regimes of whistler modes, destabilized by, respectively, the beam u_b and temperature anisotropy $A_b > 1$.

Figure 4 presents four distinct regimes of destabilized whistler modes, assuming $\delta = 0.05$, $A_c = 1.0$ and $\beta_c = \beta_p = 0.04$. In panel (a) we consider, for reference, the beam isotropic $A_b = 1.0$, and find growth or damping rates of whistlers varying only under the influence of the beam velocity u_b : the instability is obtained for higher beaming velocities $u_b = 0.5, 0.6$, and maximum growth rates are obtained for $u_b = 0.6$ (Shaaban et al., 2018a). In panel (b), for a relatively small beam anisotropy $A_b = 1.2$, growth rates are markedly stimulated by the beam velocity, and maximum growth rates are obtained for a less energetic beam, i.e., $u_b = 0.5$ (brown line). Higher anisotropies $A_b = 1.5, 2.5$ may drive an instability with significantly high growth rates (even in the absence of a beam, $u_b = 0$), see red lines in

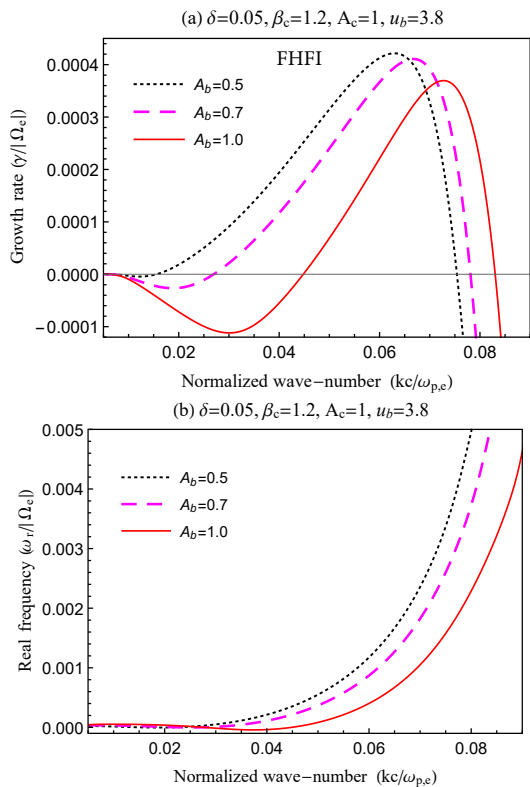


FIG. 6. FHF: The same in Figure 6 but for $A_b < 1.0$.

panels (c) and (d). In panel (c) the instability features characteristics of both the WHFI and WI, cumulating the effects of beam and temperature anisotropy. Maximum growth rates are obtained for $u_b = 0.3$. For higher anisotropies $A_b = 2.5$, in panel (d), we obtain WI-like growth rates (maximum for $u_b = 0$) which decrease as the beam velocity increases. More energetic beams, e.g., $u_b = 0.6$ (black line), may determine another transition to WHFI regime.

A series of conclusions can already be drawn, which enable to distinguish between these two regimes of unstable whistlers (also see next section of the instability thresholds). Thus, the beam anisotropy $A_b > 1.0$ stimulates the WHFI, reducing also the beam velocity required for the instability to display maximum growth rate. On the other hand, growth rates of WI are reduced by the beam, and an increase of u_b may trigger a transition to the WHFI.

IV. UNSTABLE ELECTRON FIREHOSE MODES

In this section, we investigate the LH branch of HFIs represented by the electron firehose heat-flux instability (FHF). Conditions of this instability are expected to be markedly modified under the influence of temperature anisotropies $A_{b,c} < 1$, which are responsible for the excitation of standard firehose instability (FI). For sufficiently large core plasma beta β_c and high beaming

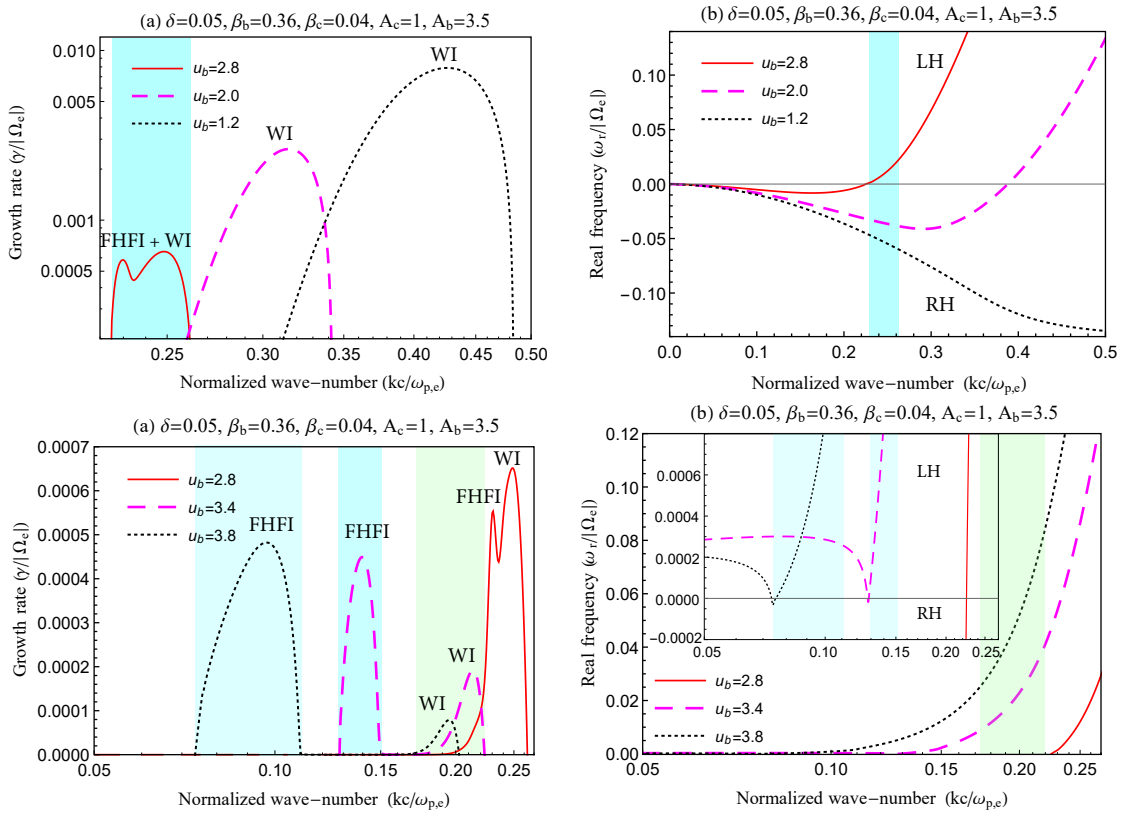


FIG. 7. Effect of the beam velocity u_b on the growth rates (panel (a)) and wave frequency (panel b) of the WI instability driven by beam anisotropy $A_b = 3.5$.

velocity $u_b > 2.7$ both the FHF and FI are expected to develop with similar dispersive features (Gary, 1993; Shaaban et al., 2018a). First we analyze the FHF under the mutual effects of the electron beam ($u_b \neq 0$) and its temperature anisotropy ($A_b \neq 1$). The unstable solutions are obtained by solving numerically the dispersion relation (5) for LH modes with ξ_p^- . By contrast to recent studies of FHF, which consider only small plasma beta regimes, i.e., $\beta_c = 0.04$ (Saeed et al., 2017b), here we assume solar wind high beta conditions, i.e., $\beta_c = \beta_p > 1$, which are more favorable to FHIs.

In Figures 5 and 6 we assume $\delta = 0.05$, $\beta_c = \beta_p = 1.2$, $A_c = 1.0$, and more energetic beams $u_b = 3.8$. Figure 5 shows the effects of an increasing anisotropy $A_b = 1.0, 1.2, 1.4$ on the FHF: in panel (a) growth rates decrease and the range of unstable wave numbers increases, and in panel (b) the wave frequency exhibits the same monotonous increasing. An opposite anisotropy $A_b = 1.0, 0.7, 0.5$, assumed in Figure 6 has a cumulative effect stimulating the FHF by increasing the growth rates and wave-frequencies. The wave frequency keeps the positive sign $\omega_r > 0$ in the range of the FHF peaks. The core anisotropy $A_c \neq 1$ manifests similar effects on the FHF (not shown here).

In the previous section we have outlined a transition from WI to WHFI, triggered by the increase of the beam speed u_b , when the temperature anisotropy of the beam is

relatively small. Here in Figure 7, we show that, provided the anisotropy is high enough, i.e., $A_b = 3.5$, WI can directly convert to FHF with increasing $u_b = 1.2, 2.0, 2.8$. The WI is driven by the beam anisotropy $A_b = 3.5$ for the same plasma parameters invoked in Saeed et al. (2017b) (their Figure 3): $\beta_c = 0.04$, $\beta_b = 0.36$, $\delta = 0.05$ and $A_c = 1.0$. Top panels present the first regime where the WI instability is dominant and the beaming velocity $u_b < 2.8$ is below but close to the threshold value for the excitation of FHF (Saeed et al., 2017b; Shaaban et al., 2018a). Increasing the beam velocity has an inhibiting effect leading to a decrease of both the growth rates and the range of unstable wave numbers of WI (panel a). The corresponding wave frequencies (panel b) decrease and remain RH polarized ($\omega_r < 0$) in the range of the WI instability peaks, unless for energetic beams when the polarization changes to LH (cyan areas) under the influence of FHF which exhibit a second distinct peak of growth rates (red solid line). The double-peak growth rates is relevant for the transition between the two regimes of FHF and WI. FHF becomes dominant for more energetic beams ($u_b > 2.8$), when the FHF peak is markedly enhanced moving towards lower wave-numbers (bottom panels c and d). Small peaks of WI are decoupled and still visible, but remain LH polarized (green area). Such reversals of the whistler mode polarizations have been observed by STEREO in the Earth's inner plasma-sphere

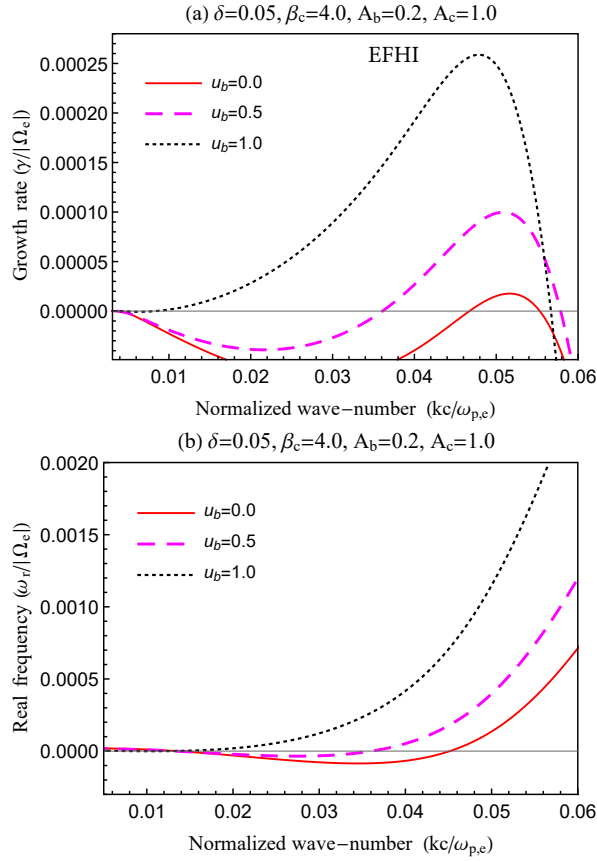


FIG. 8. Effect of the beam velocity u_b on the growth rates (panel a) and wave frequency (panel b) of the EFHI driven by beam anisotropy $A_b = 0.2$.

at $L < 2$ (Breneman et al., 2011).

For a core with a sufficiently large plasma beta, a beam with an excess of parallel temperature, i.e., $A_b < 1$ may excite the electron firehose (EFH) instability. Figure 8 shows the effect of the beam velocity u_b on the EFH instability driven by a temperature anisotropy $A_b = 0.2$ for the following plasma parameters $\delta = 0.05$, $\beta_c = \beta_p = \beta_b/10 = 4.0$, $A_c = 1.0$. The growth rates (panel a) and wave frequencies (panel b) of EFH instability are significantly stimulated by increasing $u_b = 0.0, 0.5, 1.0$. These effects contrast with the inhibition of WI shown in Figure 7.

V. THRESHOLD CONDITIONS

Thresholds offer a concise but more comprehensive picture of the unstable regimes. Figures 9–11 present the instability thresholds derived for a small maximum growth rate $\gamma_m = 2 \times 10^{-4}|\Omega_e|$, approaching marginal stability, i.e. $\gamma_m \rightarrow 0$. These thresholds are derived in terms of the instability drivers, i.e., beam velocity u_b or temperature anisotropy A_b , as a function of the core plasma beta β_c . The other plasma parameters are kept constant, e.g.,

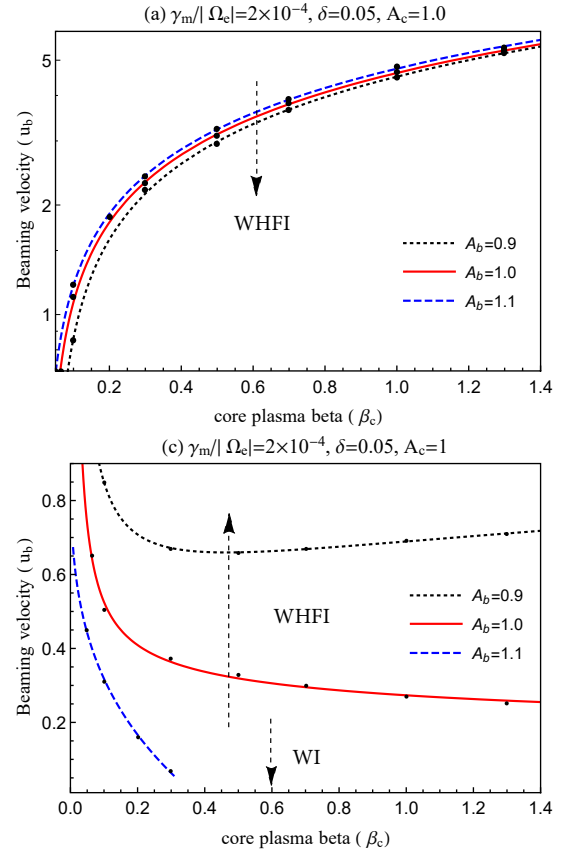


FIG. 9. Effect of the beam anisotropy A_b on the (a) upper and (b) lower thresholds ($\gamma_m = 2 \times 10^{-4}|\Omega_e|$) of the WHFI.

$\delta = 0.05$ and $A_c = 1.0$. Mathematically, the instability thresholds are fitted to a function of β_c generically expressed by (Shaaban et al., 2016)

$$\Delta = \left(1 + \frac{a}{\beta_c^b}\right) \frac{c}{\beta_c^d} \quad (6)$$

where

$$\Delta = \begin{cases} A_b, & \text{for temperature anisotropy instabilities} \\ u_b, & \text{for heat flux instabilities.} \end{cases}$$

Fitting parameters a , b , and c are tabulated in Tables II–IV in Appendix.

As shown in Figure 4 (a), the WHFI growth rates vary non-uniformly with increasing the beaming velocity, suggesting, as also shown recently by Shaaban et al. (2018a), that the unstable WHF modes are bounded between two thresholds of the beam velocity. Figure 9 describes the effect of temperature anisotropy $A_b \neq 1.0$ on the upper and lower thresholds of WHFI, in panels (a) and (b), respectively. We contrast thresholds for an isotropic beam ($A_b = 1$, solid-red), with those for $A_b = 1.1$ (dashed-blue) and $A_b = 0.9$ (dotted-black). In panel (a) the upper threshold is slightly increased by the anisotropy in perpendicular direction, $A_b = 1.1$, but it is slightly

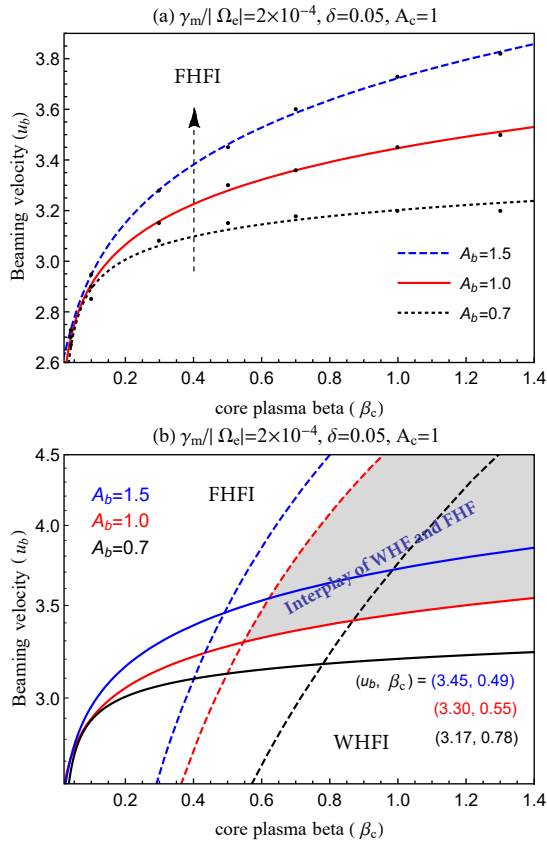


FIG. 10. Effect of the beam anisotropy A_b on the (a) FHF threshold and a comparison with the (b) WHFI upper threshold for $\gamma_m = 2 \times 10^{-4} |\Omega_e|$.

decreased by an opposite anisotropy in parallel direction, $A_b = 0.9$. Only small variations are obtained in this case, given that this regime of WHFI is mainly controlled by relatively high beaming velocities, and temperature anisotropies are relatively small. However, for the same anisotropies, in panel (b) the lower WHFI threshold undergoes more important changes. This threshold is markedly enhanced for $A_b = 0.9$, and this difference is increased with increasing the core plasma beta β_c , squeezing the unstable regime of WHFI (upper directed arrow). In an opposite situation for $A_b = 1.1$, the lower WHFI threshold is markedly reduced to lower beaming velocities u_b , and with increasing β_c the WI peak starts to dominate the WHFI peak, which finally quenches completely. This regime marks the transition from WHFI to the most common WI (lower directed arrow) which becomes exclusively driven by the temperature anisotropy (for $u_b = 0$ and $\beta > \beta_c \simeq 0.3$).

Figure 10 (a) describes the effect of temperature anisotropy on the FHF thresholds, by contrasting thresholds derived for an isotropic beam ($A_b = 1$, solid-red) with the those for $A_b > 1.0$ (dashed-blue) and $A_b < 1.0$ (dotted-black). Variations in this case resemble those of the WHFI upper threshold, but the most unstable FHF modes are situated above the thresh-

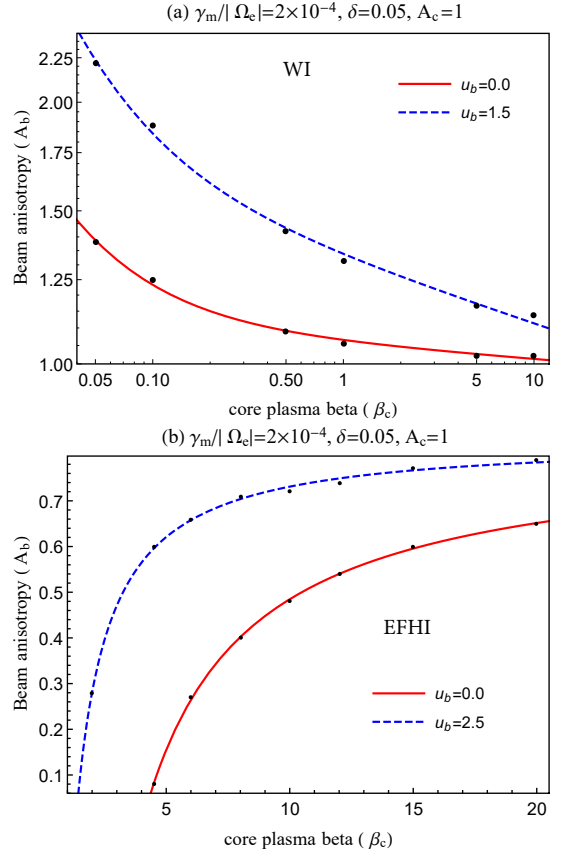


FIG. 11. Effect of the beam velocity u_b on WI (panel a) and EFH (panel b) instabilities thresholds with maximum growth rates $\gamma = 2 \times 10^{-4} |\Omega_e|$. The plasma parameters are mentioned in each panel.

olds, as pointed out by the dashed arrow. Temperature anisotropy $A_p = 1.5$ has a stimulating effect on the FHF threshold, squeezing the unstable regime of the FHF modes, while for $A_b = 0.7$ the threshold is reduced and the FHF regime is enlarged. These effects are boosted by increasing β_c , confirming the results in Figures 5 and 6. For the sake of comparison, in panel (b) we compare the FHF and the WHFI thresholds for the same set of plasma parameters ($\delta = 0.05$, $A_c = 1.0$), and different anisotropies $A_b = 0.7, 1.0, 1.5$. As shown in panel (a), the unstable FHF modes require relatively high beaming velocities $u_b > 2.7$ making the comparison relevant only for the WHFI upper threshold. For isotropic beams (red lines) the FHF is dominant at low $\beta_c < 0.55$ and high $u_b > 2.7$, and also at beaming velocities exceeding the WHFI (upper) threshold, while the WHFI is dominant for less energetic beams with $u_b < 2.7$. If $u_b > 3.3$ and $\beta_c > 0.55$ are high enough, we can identify a regime of transition (gray shaded regime) where the unstable FHF and WHF modes may co-exist and interplay. The anisotropic beams with $A_b = 1.5$ determine the interplay regime to move towards higher $u_b > 3.45$ and lower limit $\beta_c > 0.49$. For an opposite anisotropy $A_b > 0.7$ this regime moves towards lower $u_b > 3.17$ and higher limit

$\beta_c > 0.78$.

In order to complete the analysis, in Figure 11 we describe the effect of the beam velocity on the thresholds of temperature anisotropy driven instabilities, WI in panel (a) and FI in panel (b). As expected, the WI threshold is markedly enhanced by the beam velocity $u_b = 1.5$, confirming the inhibiting effect already shown on the growth-rates in Figures 3 and 7. Here we can see that this effect is reduced with increasing β_c . Also expected is the effect shown by the EFH threshold, which is markedly reduced in the presence of beam, see panel (b), confirming the stimulating effect of beams on the EFHI growth rates, obtained in Figure 8.

VI. DISCUSSIONS AND CONCLUSIONS

As shown in the introduction, the heat-flux instabilities may play a major role in the evolution of electron beams in the solar wind, but a definitive answer on this issues requires a detailed examination of these instabilities in conditions specific to space plasmas. The kinetic approach proposed in this paper enables an advanced characterization of the heat-flux instabilities for complex but realistic conditions, when the electron beams exhibit temperature anisotropies. The new unstable regimes uncovered here are controlled by two drivers, i.e., beaming velocity u_b and beam anisotropy A_b , and by the core plasma beta β_c , and we have contrasted with idealized regimes of instabilities driven either by isotropic beams (Saeed et al., 2017a; Shaaban et al., 2018a) or by non-drifting (core-beam) populations with temperature anisotropies.

For less energetic beams the WHFI is found to be very sensitive to the beam anisotropy: growth rates are markedly increased if $A_b > 1.0$, and are decreased when $A_b < 1.0$ (Figure 1). Core anisotropy $A_c \neq 1.0$ shows similar effects on the WHFI, but it is much less effective than the beam anisotropy, see Figure 2. The common WI can be excited at low $\beta_c < 1$ but for a significant $A_b > 1.0$. The beam has an inhibiting effect on the WI: reducing growth rates and the range of unstable wave-numbers with increasing the beaming velocity. But, apparently, the beam may stimulate WI driven by the core anisotropy is $A_c > 1.0$, see Figure. 3, where growth rates increase and saturate for higher beaming velocities, resembling a regime characteristic to WHFI.

Firehose instabilities are expected to develop for relatively higher u_b or/and higher β_c , and contrary to whistlers, differences between FHFI and FI are easier to determine. FHFI can be excited even for a low $\beta_c < 1$, provided the beam velocity is high enough, while FI requires a high $\beta_c \geq 3.0$ and a temperature anisotropy $A_b < 1.0$. For a moderately high $\beta_c = 1.2$, we have found that $A_b < 1$ has a stimulating effect on the FHFI, increasing the growth rates and the corresponding wave frequencies (Figure 5). The anisotropy in perpendicular direction has an opposite effect, see Figure 6, where growth rates and wave frequencies of FHFI decrease with

increasing $A_b > 1$. These variations of the growth rates and wave frequencies with the temperature anisotropies have not been observed in the previous studies which were restricted to low $\beta_c = 0.04$ regimes (Saeed et al., 2017b).

Figure 7 suggests that, depending on the beaming velocity u_b , the interplay with temperature anisotropy $A_b > 1.0$ can be divided into two distinct regimes. For a beaming velocity below the threshold of FHFI, i.e., $u_b < 2.8$, dominant is the WI, and, as expected, the beam has an inhibiting effect, reducing the growth rates and the range of unstable wave-numbers. In the second regime, more energetic beams with $u_b \geq 2.8$ excite the FHFI and the growth rates display a second distinct peak at low wave-numbers. The beam stimulates the FHFI, but inhibits the WI peak, and wave frequencies may change sign showing a LH polarization even in the range of the WI peak, under the influence of a dominant FHFI. Regarding the more common FHI driven by an excess of parallel temperature ($A < 1$), the effective free energy is enhanced in the presence of a beam, and FHI is stimulated (Figure 8). Another remark can be made if we calculate the core drift velocity u_c for the same plasma parameters used to derive the heat-flux unstable modes in Figures 4 (a) and 7 (b). The plasma parameters used for the WHFI, e.g., $\delta = 0.05$, $\beta_c = 0.04$, and $u_b = U_b/c \omega_e/|\Omega_e| = 0.6$, where $\omega_e/|\Omega_e| = 100$, imply for the core drift velocity $U_c = \delta U_b/(1 - \delta) = 3.16 \times 10^{-4}$, which is about 1.6 times higher than Alfvén velocity $V_A = 2 \times 10^{-4}c$, commonly invoked in similar studies. For the FHFI we assumed $\delta = 0.05$, $\beta_c = 0.04$ and $u_b = 3.8$, implying a higher core drift velocity $U_c = 10 V_A$. In the solar wind U_c is comparable to, or larger (three times larger in a collisionless plasma) than V_A (Pulupa et al., 2014). Thus, our results strengthen the early predictions (Gary et al., 1975; Gary and Li, 2000) that whistler instabilities could be more efficient in regulating the electron heat flux in the solar wind.

Thresholds displayed in Figures 9–11 may provide a better overview on the interplay of these instabilities. In Fig. 9 the unstable WHF modes are located between two thresholds, namely, a lower and an upper threshold. In terms of the beam velocity u_b , the interval of WHFI in between these two thresholds may significantly increase even for a modest temperature anisotropy in perpendicular direction $A_b > 1$, or it is markedly reduced by an opposite anisotropy in parallel direction $A_b < 1$. Situated above these thresholds, the unstable regime of the FHF modes, see Figure 10 (a), show opposite effects, increasing when $A_b < 1$ and diminishing for $A_b > 1$. All these variations increase with increasing β_c . In Figure 10 (b), we have identified unstable regimes conditioned by both the WHFI and FHFI, which move either towards higher u_b and lower β_c if the anisotropy increases in perpendicular direction ($A_b > 1$), or towards lower u_b and higher β_c by increasing the anisotropy in parallel direction ($A_b < 1.0$). These unstable regimes are con-

siderably enhanced by increasing β_c . In Figure 11 we have described the effects of beam on the temperature anisotropy thresholds. The WI threshold is increased by increasing the beaming velocity, confirming the inhibiting effect on the growth rates in Figures 3 and 7. On the other hand, the FI threshold is decreased by increasing the beaming velocity, confirming the stimulating effect on the growth rates in Figure 8.

To conclude, we have identified new regimes of the whistler and firehose unstable modes, which are highly conditioned by the interplay of two sources of free energy, an electron beam and its intrinsic temperature anisotropy. Present study is focused on parallel electromagnetic modes, with intention to facilitate the analysis and differentiate between different regimes of these instabilities. In the oblique directions very efficient may be the aperiodic instabilities, like electron mirror or electron firehose, but their properties are known only for regimes triggered by the temperature anisotropies (Maneva et al., 2016; Shaaban et al., 2018b). Our results should therefore stimulate further investigations to address the full spectrum of beam-driven electromagnetic and electrostatic instabilities.

ACKNOWLEDGMENTS

The authors acknowledge support from the Katholieke Universiteit Leuven, Ruhr-University Bochum. These results were obtained in the framework of the projects SCHL 201/35-1 (DFG-German Research Foundation), GOA/2015-014 (KU Leuven), G0A2316N (FWO-Vlaanderen), and C 90347 (ESA Prodex 9). S.M. Shaaban would like to acknowledge the support by a Postdoctoral Fellowship (Grant No. 12Z6218N) of the Research Foundation Flanders (FWO-Belgium) and the support by a Travel Grant for a long stay aboard (Grant No. V419818N) of FWO-Belgium. P.H.Y. acknowledges NSF grant AGS1550566 to the University of Maryland, the Science Award Grant from the GFT Charity, Inc., to the University of Maryland, and the BK21 plus program from the National Research Foundation (NRF), Korea, to Kyung Hee University. Some basic ideas developed in this paper have been discussed at the 1st ISSI meeting of the international team: Kappa Distributions.

Appendix A: Fitting parameters in Eq. (6)

We have used Eq. (6) to describe the instability plasma conditions in terms of the instability thresholds from Figures 9–11, defined by either the beam velocity or the temperature anisotropy (two distinct drivers), as a function of the core plasma beta. The fitting parameters a , b , c , and d are tabulated in Tables II and III for the heat flux instabilities (WHFI and FHFI), and in Table IV for the anisotropy driven instabilities (WI and FI).

Breneman, A., Cattell, C., Wygant, J., Kersten, K., Wilson, L. B., Schreiner, S., Kellogg, P. J. and Goetz, K.

TABLE II. Fitting parameters in Figure 9

A_b	WHFI (a)			WHFI (b)		
	0.9	1.0	1.1	0.9	1.0	1.1
a	0.13	0.03	-1.32	-0.023	-0.04	-0.01
b	1.0	1.0	-0.29	1.0	1.0	1.0
c	0.30	0.26	0.0	4.72	4.67	4.81
d	-0.22	0.18	1.0	-0.52	-0.54	-0.53

TABLE III. Fitting parameters in Figure 10

A_b	FHFI			WHFI		
	0.7	1.0	1.5	0.7	1.0	1.5
a	-0.003	2.45	2.72	5.82	-0.023	-0.008
b	1.0	-0.1	-0.14	1.0	1.0	1.0
c	3.21	0.0	0.0	0.55	4.72	5.11
d	-0.03	1.0	1.0	-1.54	-0.52	-0.53

- (2011), ‘Large-amplitude transmitter-associated and lightning-associated whistler waves in the Earth’s inner plasmasphere at $L < 2$ ’, *Journal of Geophysical Research: Space Physics* **116**(6), 1–10.
- Fried, B. and Conte, S. (1961), ‘The plasma dispersion function’, *The Plasma Dispersion Function*, New York: Academic Press, 1961.
- Gary, S. P. (1985), ‘Electromagnetic electron beam instabilities: Hot, isotropic beams’, *Journal of Geophysical Research* **90**(A11), 10815.
- Gary, S. P. (1993), *Theory of Space Plasma Microinstabilities*, Cambridge University Press.
- Gary, S. P., Feldman, W. C., Forslund, D. W. and Montgomery, M. D. (1975), ‘Heat flux instabilities in the solar wind’, *Journal of Geophysical Research* **80**(31), 4197–4203.
- Gary, S. P. and Li, H. (2000), ‘Whistler Heat Flux Instability at High Beta’, *The Astrophysical Journal* **529**(2), 1131–1135.
- Gary, S. P. and Saito, S. (2007), ‘Broadening of solar wind strahl pitch-angles by the electron/electron instability: Particle-in-cell simulations’, *Geophysical Research Letters* **34**(14).
- Gary, S. P. and Wang, J. (1996), ‘Whistler instability: Electron anisotropy upper bound’, *Journal of Geophysical Research: Space Physics* **101**(A5), 10749–10754.
- Lacombe, C., Alexandrova, O., Matteini, L., Santolík, O., Cornilleau-Wehrin, N., Mangeney, A., de Conchy, Y. and Maksimovic, M. (2014), ‘Whistler mode waves and the electron heat flux in the solar wind: Cluster observations’, *The Astrophysical Journal* **796**(1), 5.
- Lazar, M., Shaaban, S. M., Fichtner, H. and Poedts, S. (2018), ‘Temperature anisotropy instabilities stimulated by the interplay of the core and halo electrons in space plasmas’, *Physics of Plasmas* **25**(2), 022902.
- Lengyel-Frey, D., Hess, R., MacDowall, R., Stone, R., Lin, N., Balogh, A. and Forsyth, R. (1996), ‘Ulysses observations of whistler waves at interplanetary shocks and in the solar wind’, *Journal of Geophysical Research: Space Physics* **101**(A12), 27555–27564.
- Lin, N., Kellogg, P., MacDowall, R., Scime, E., Balogh, A., Forsyth, R., McComas, D. and Phillips, J. (1998), ‘Very low frequency waves in the heliosphere: Ulysses observations’, *Journal of Geophysical Research: Space Physics* **103**(A6), 12023–12035.
- Maksimovic, M., Zouganelis, I., Chaufray, J.-Y., Issautier, K., Scime, E., Littleton, J., Marsch, E., McComas, D., Salem, C., Lin, R. et al. (2005), ‘Radial evolution of the electron distribution functions in the fast solar wind between 0.3 and 1.5 au’, *Journal of Geophysical Research: Space Physics* **110**(A9).

TABLE IV. Fitting parameters in Figure 11

u_b	WI		FI	
	0.0	1.5	0.0	2.5
a	0.012	0.018	-4.0	-1.34
b	1.0	1.0	1.0	1.0
c	1.05	1.32	0.80	0.85
d	0.017	0.072	-0.004	0.006

- Maneva, Y., Lazar, M., Vinas, A. and Poedts, S. (2016), ‘Mixing the solar wind proton and electron scales: effects of electron temperature anisotropy on the oblique proton firehose instability’, *The Astrophysical Journal* **832**(1), 64.
- Paesold, G. and Benz, A. O. (1999), ‘Electron firehose instability and acceleration of electrons in solar flares’, *Astronomy Astrophysics* **351**(astro-ph/0001262), 741–746.
- Pagel, C., Gary, S. P., de Koning, C. A., Skoug, R. M. and Steinberg, J. T. (2007), ‘Scattering of suprathermal electrons in the solar wind: ACE observations’, *Journal of Geophysical Research (Space Physics)* **112**, A04103.
- Phillips, J., Gosling, J., McComas, D., Bame, S., Gary, S. and Smith, E. (1989), ‘Anisotropic thermal electron distributions in the solar wind’, *Journal of Geophysical Research: Space Physics* **94**(A6), 6563–6579.
- Pierrard, V., Lazar, M., Poedts, S., Štverák, Š., Maksimovic, M. and Trávníček, P. (2016), ‘The electron temperature and anisotropy in the solar wind. comparison of the core and halo populations’, *Solar Physics* **291**(7), 2165–2179.
- Pilipp, W., Miggenrieder, H., Montgomery, M., Mühlhäuser, K.-H., Rosenbauer, H. and Schwenn, R. (1987), ‘Characteristics of electron velocity distribution functions in the solar wind derived from the helios plasma experiment’, *Journal of Geophysical Research: Space Physics* **92**(A2), 1075–1092.
- Pulupa, M. P., Bale, S. D., Salem, C. and Horaites, K. (2014), ‘Spin modulated spacecraft floating potential: Observations and effects on electron moments’, *Journal of Geophysical Research: Space Physics* **119**(2), 647–657.
- Saeed, S., Sarfraz, M., Yoon, P. H., Lazar, M. and Qureshi, M. N. S. (2017a), ‘Electron heat flux instability’, *Monthly Notices of the Royal Astronomical Society* **465**(2), 1672–1681.
- Saeed, S., Sarfraz, M., Yoon, P. H. and Qureshi, M. N. S. (2017b), ‘Characteristics of heat flux and electromagnetic electron-cyclotron instabilities driven by solar wind electrons’, *Monthly Notices of the Royal Astronomical Society* **493**6, stx049.
- Saito, S. and Gary, S. P. (2007), ‘Whistler scattering of suprathermal electrons in the solar wind: Particle-in-cell simulations’, *Journal of Geophysical Research (Space Physics)* **112**, A06116.
- Shaaban, S., Lazar, M., Astfalk, P. and Poedts, S. (2018b), ‘Stimulated mirror instability from the interplay of anisotropic protons and electrons, and their suprathermal populations’, *Journal of Geophysical Research: Space Physics* **123**(3), 1754–1766.
- Shaaban, S., Lazar, M., Poedts, S. and Elhanbaly, A. (2016), ‘The interplay of the solar wind proton core and halo populations: Emic instability’, *Journal of Geophysical Research: Space Physics* **121**(7), 6031–6047.
- Shaaban, S. M., Lazar, M. and Poedts, S. (2018a), ‘Clarifying the solar wind heat-flux instabilities’, *Monthly Notices of the Royal Astronomical Society* p. sty1567.
URL: doi.org/10.1093/mnras/sty1567
- Štverák, Š., Maksimovic, M., Trávníček, P. M., Marsch, E., Fazakerley, A. N. and Scime, E. E. (2009), ‘Radial evolution of non-thermal electron populations in the low-latitude solar wind: Helios, Cluster, and Ulysses Observations’, *Journal of Geophysical Research (Space Physics)* **114**, A05104.
- Štverák, Š., Trávníček, P., Maksimovic, M., Marsch, E., Fazakerley, A. N. and Scime, E. E. (2008), ‘Electron temperature anisotropy constraints in the solar wind’, *Journal of Geophysical Research (Space Physics)* **113**, A03103.
- Viñas, A., Gurgiolo, C., Nieves-Chinchilla, T., Gary, S. and Goldstein, M. (2010), Whistler waves driven by anisotropic strahl velocity distributions: Cluster observations, in ‘AIP Conference Proceedings’, Vol. 1216, AIP, pp. 265–270.
- Vocks, C., Salem, C., Lin, R. P. and Mann, G. (2005), ‘Electron Halo and Strahl Formation in the Solar Wind by Resonant Interaction with Whistler Waves’, *The Astrophysical Journal* **627**, 540–549.